SZ scaling relations in Galaxy Clusters: results from hydrodynamical N–body simulations

António J. C. da Silva
LAOMP, 14, Av. Edouard Belin, 31400 Toulouse, France

Abstract. Observations with the SZ effect constitute a powerful new tool for investigating clusters and constraining cosmological parameters. Of particular interest is to investigate how the SZ signal correlates with other cluster properties, such as the mass, temperature and X-ray luminosities. In this presentation we quantify these relations for clusters found in hydrodynamical simulations of large scale structure and investigate their dependence on the effects of radiative cooling and pre-heating.

Keywords: galaxy clusters, cosmic microwave background

1. Introduction

Galaxy clusters are the largest gravitationally bound objects in the Universe. They have typical masses of $10^{14} - 10^{15} h^{-1}$ $M_\odot$ and contain hundreds of galaxies within radius of a few Mpc. The intra-cluster medium (ICM) is filled with hot ionized gas, typically at temperatures 1–15 keV, which produces strong X-ray emission and causes spectral distortions in the CMB spectrum via the Sunyaev–Zel'dovich (SZ) effect (see Ref. [11]).

Numerical simulations indicate that the non-baryonic dark matter component in clusters, which is the dominant fraction of their mass, is remarkably self-similar for systems in approximate state of equilibrium, see e.g. Ref. [8]. However, the baryonic gas component does not share the same degree of self-similarity. This is more evident from observations of the L_X–T relation in clusters, which is much steeper than is predicted by simple self-similar scaling laws, specially for low-mass systems (see e.g. Refs. [4, 14]). This deviation from self-similarity has been interpreted as due to non-gravitational processes, such as radiative cooling and heating, that raise the entropy of the gas, see e.g. Ref. [10].

The purpose of this study is to investigate the correlation between intrinsic properties of clusters found in simulations, and to compare them with analytical scaling laws. We use high-resolution hydrodynamical simulated clusters to assess the impact of radiative cooling and pre-heating on these scaling relations. Here we focus only on scalings involving the SZ integrated signal, Y, at redshift zero. The effects on the mass–temperature and X-ray scaling relations have already been analyzed in detail in Refs. [6, 7] for this same set of simulations. A more

detailed analysis of the SZ scaling relations can be found in Ref. [2], whose results supersede those presented at this conference.

2. Scaling relations in Clusters

The quantity we want to study is the total thermal SZ flux density received from a cluster. This is defined as the integral of the thermal SZ specific intensity (described by the y Comptonization parameter) over the solid angle occupied by the source in the sky. More exactly, we want to investigate how the frequency-independent SZ flux,

$$Y \equiv \int y \, d\Omega = d_A^{-2} \int y \, dA = \frac{k_B \sigma_{\rm T}}{mc^2} \, d_A^{-2} \int_V T_{\rm e} n_{\rm e} \, dV \, , \qquad (1)$$

correlates with other cluster properties. This is known as the SZ integrated Y-flux or Y-luminosity. Note that d_A is the angular diameter distance, $dA = d\Omega \, d_A^{-2}$ is the sky projected area of the source and the last integral is performed over the volume of the cluster. Since y is dimensionless, Y has dimensions of a solid angle. Equation (1) indicates that Y is proportional to the mean electron temperature, $\langle T_{\rm e} \rangle$, and the total cluster mass, M,

$$Y \propto f_{\rm gas} \, \langle T_{\rm e} \rangle \, M \, d_A^{-2}, \qquad (2)$$

where $f_{\rm gas}$ is the gas mass fraction of the cluster. Note that $\langle T_{\rm e} \rangle$ is the mass (or particle) weighted temperature, which may differ from the *emission-weighted* temperature measured in X-ray observations.

The dependence of the X-ray bolometric luminosity on mass and temperature follows from its definition,

$$L_X = \int_V \frac{\rho_{\rm gas}^2}{(\mu m_{\rm p})^2} \Lambda(T) \, dV \, . \qquad (3)$$

The integral is over the volume of the cluster, $\mu m_{\rm p} \simeq 1 \times 10^{-24}$ is the mean mass per particle, $\Lambda(T)$ is the gas cooling function and $\rho_{\rm gas}$ is the gas density. Assuming the gas is well described by an isothermal temperature profile one obtains,

$$L_X \propto f_{\rm gas}^2 \, M \, \Delta_{\rm c} \, \rho_{\rm crit} \, \Lambda(T) \; \propto f_{\rm gas}^2 \, M \, \Delta_{\rm c} \, \rho_{\rm crit} \, T^{1/2} \, , \qquad (4)$$

where the last step results from assuming that the bolometric luminosity in clusters is dominated by bremsstrahlung emission, $\Lambda \propto T^{1/2}$.

As suggested by the virial theorem the mass and the temperature of a cluster are tightly correlated quantities. At the virial radius these

are related by the virial relation, $k_{\rm B}T \propto GM/r$. The mass enclosed within this radius can be written as $M = 4\pi\, r^3\, \Delta_{\rm c}\, \rho_{\rm crit}/3$, where $\Delta_{\rm c}$ is the overdensity contrast between the mean cluster density within r and the critical density, $\rho_{\rm crit}$. Using this expression one obtains

$$T \propto M^{2/3}\, (\Delta_{\rm c}\, \rho_{\rm crit})^{1/3} \propto \left(\frac{\Delta_{\rm c}}{\Omega(z)}\right)^{1/3} M^{2/3}\, (1+z)\,. \qquad (5)$$

Using Eq. (5) into Eqs. (2) and (4), with $\langle T_{\rm e}\rangle \sim T$, one can derive general scaling relations for the SZ and X-ray luminosities as a function of cosmology, redshift, and the cluster mass (or temperature). According to these, clusters are expected to present the following interdependencies of mass, temperature, X-ray luminosities and integrated SZ fluxes at redshift zero:

$$T \propto M^{2/3}\,, \quad L_X \propto M^{4/3} \propto T^2\,, \quad Y \propto M^{5/3} \propto T^{5/2} \propto L_X^{5/4}\,. \qquad (6)$$

These expressions coincide with the scaling relations predicted by the self-similar model [5], which is expected to describe well the correlation between the above properties if shock heating from gravitational collapse is the dominant mechanism driving the gas evolution.

3. Simulations, Cluster identification and catalogues

We present results from three simulations of a single ΛCDM cosmology with density parameter, $\Omega_{\rm m} = 0.35$, cosmological constant, $\Omega_\Lambda = 0.65$, Hubble parameter $h = 0.71$, baryon density, $\Omega_{\rm B}h^2 = 0.019$, shape parameter of the CDM power spectrum, $\Gamma = 0.21$, and normalization $\sigma_8 = 0.9$. We use 160^3 particles of each gas and dark matter in a box of side $100\,h^{-1}$Mpc, which gives particle masses of $m_{\rm gas} = 2.6\times10^9\, h^{-1}{\rm M}_\odot$ and $m_{\rm dark} = 2.1\times10^{10}\, h^{-1}{\rm M}_\odot$ respectively. The gravitational softening at redshift zero was $25\,h^{-1}$kpc. The simulations were carried out as part of the Virgo Consortium program, using a parallel version of the `hydra` N-body/hydrodynamics code (see Refs. [1, 9]).

The first of the three simulations was performed without any additional heating or cooling mechanisms; we refer to this as the 'non-radiative' simulation. The second simulation included a model for radiative cooling using the method described in Ref. [13], except that we adopted the cooling tables of Ref. [12] and a global gas metallicity evolving as $Z = 0.3(t/t_0)Z_\odot$, where $Z_\odot$ is the solar metallicity and t/t_0 is the cosmic time in units of its present value. Our third simulation, which also includes cooling, was performed in order to study the effects of pre-heating the gas at high redshift. We considered an energy

injection of 0.1 keV per gas particle at redshift four for this run. Note that this is less energy injected per particle than that used in the pre-heating run of Ref. [2] (1.5 keV). We used identical initial conditions to enable direct comparisons between clusters forming in the three runs. For more details see Ref. [3].

In simulations clusters are identified with a spherical overdensity group finder algorithm, as described in Ref. [6]. The identification process consists of several steps. The first is to create a minimal-spanning tree of all dark-matter particles whose density exceeds $\delta = 178 \times \Omega^{-0.55}(z)$ times the mean dark-matter density in the box. The next step is to split the minimal-spanning tree into clumps of particles using a maximum linking length equal to $0.5\delta^{-1/3}$ times the mean inter-particle separation. Then we grow a sphere around the centre of the clump until the enclosed mean density is Δ times larger then the comoving critical density. Because the density parameter of the real universe is not known, we have chosen to average the properties within an isodensity contour of $\Delta = 200$, corresponding to a radius r_{200}. A final cluster catalogue is produced by selecting objects whose total mass is equivalent to at least 500 particles of gas and dark matter within this radius, and whose centre is not located within a more massive cluster. In this way our catalogues (available online from `virgo.sussex.ac.uk`) are complete in mass down to $M_{\rm lim} \approx 1.18 \times 10^{13} h^{-1} M_{\odot}$.

For each cluster the catalogues contain several entries representing different cluster properties. Relevant for this study are the bolometric luminosity, $L_{\rm bol} = \sum m_i \, \rho_i \, \Lambda(T_i, Z)/(\mu m_{\rm p})^2$, the emission-weighted temperature, $T_{\rm ew} = \sum m_i \, \rho_i \Lambda(T_i, Z) \, T_i / \sum m_i \, \rho_i \Lambda(T_i, Z)$, the mass-weighted temperature $T_{\rm mw} = \sum m_i \, T_i / \sum m_i$, and the hot gas mass fraction, $f_{\rm gas} = \sum m_i / M$. In these expressions, summations run over gas particles with temperatures above $10^5 \, (1 + z)^2$ K (i.e. the hot intra-cluster gas that gives rise to the SZ and X-ray emission) within a radius r_{200}. M is the total mass, i.e., the sum of the mass of all particles, including both baryons and dark matter, within the same radius. The quantities, m_i, T_i, ρ_i and $\Lambda(T_i, Z)$ are respectively the mass, temperature, density and emissivity (cooling function) of the particles.

The intrinsic SZ luminosity, defined as $Y^{\rm int} = Y \, d_A(z)^2$, can then be computed from the cluster catalogues as,

$$Y^{\rm int} = \frac{\sigma_{\rm T} \, k_{\rm B}}{m_{\rm e} c^2} \, \frac{(1 + X)}{2 m_{\rm p}} \sum_{i \in {\rm hgas}} m_i \, T_i = \frac{\sigma_{\rm T} \, k_{\rm B}}{m_{\rm e} c^2} \, \frac{0.88}{m_{\rm p}} \, f_{\rm gas} \, T_{\rm mw} \, M \, , \qquad (7)$$

where we assume a hydrogen mass fraction of $X = 0.76$. Since the y-parameter is dimensionless we will quote $Y^{\rm int}$ in units of $(h^{-1}{\rm Mpc})^2$.

4. Results: scaling relations at redshift zero

In Figure 1 we plot the intrinsic SZ-flux against mass (top panel), mass-weighted temperature (centre panel) and X-ray luminosity (bottom panel), for clusters found in simulation boxes at redshift zero. All properties are calculated within r_{200}. For the plots in this paper we adopt the following convention: gray crosses represent clusters from the non-radiative simulation, whereas dark gray and light gray crosses illustrate the properties of clusters in the cooling and pre-heating runs. To ensure completeness in temperature and luminosity we have trimmed the original cluster catalogues in the two bottom plots by selecting only clusters with emission-weighted temperatures above 0.35, 0.75 and 0.55 keV for the non-radiative, cooling and pre-heating simulations, respectively. This permits to avoid the introduction of artificial trends on the derived fittings for the $Y_{200}^{\rm int} - T_{\rm mw}$ and $Y_{200}^{\rm int} - L_{\rm bol}$ relations.

The plots show that $Y_{200}^{\rm int}$ is tightly correlated with mass and the mass-weighted temperature in all runs. The correlation between the SZ integrated flux and the X-ray luminosity is also strong, but shows significantly more scatter. This is because the X-ray emission is sensitive to the gas distribution and temperature, whereas $Y_{200}^{\rm int}$ is essentially a function of the total thermal energy of the hot gas mass within r_{200}. In each plot, the solid lines are power-law best fits to distribution of clusters in each simulation. For the $Y_{200}^{\rm int} - M_{200}$ correlation we find the following best-fit parameters for each simulation run:

Non-radiative: $Y_{200}^{\rm int} = 1.2 \times 10^{-6}\ (M_{200}/M_{14})^{1.7}\ \left(h^{-1}\,{\rm Mpc}\right)^2$

Cooling: $Y_{200}^{\rm int} = 8.3 \times 10^{-7}\ (M_{200}/M_{14})^{1.8}\ \left(h^{-1}\,{\rm Mpc}\right)^2$

Pre-heating: $Y_{200}^{\rm int} = 1.0 \times 10^{-6}\ (M_{200}/M_{14})^{1.7}\ \left(h^{-1}\,{\rm Mpc}\right)^2$,

where $M_{14} = 10^{14}\,h^{-1}\,{\rm M}_\odot$. The slope from the non-radiative run reproduces well the value 5/3 predicted by the self-similar scaling Eq. (6). The cooling simulation presents a steeper slope and lower normalization then the other two runs. This implies significant differences in $Y_{200}^{\rm int}$, particularly for low-mass systems. For example, at $M_{200} \sim 10^{13}\,h^{-1}\,{\rm M}_\odot$, sources in the cooling simulation are about two times less strong then their non-radiative counterparts. At $10^{14}\,h^{-1}\,{\rm M}_\odot$ the relative difference is still of about 50 percent, but gets much reduced at higher masses.

The differences between runs can be explained in terms of the changes caused by our models of cooling and pre-heating in the hot gas fraction and mass-weighted temperature of clusters. The inclusion of cooling in both radiative simulations lowers the hot gas mass fraction and tends to increases the emission-weighted temperature due to the removal of cooled material from the hot gas phase. The increase in temperature results from the infall of high-entropy gas which replaces the cooled

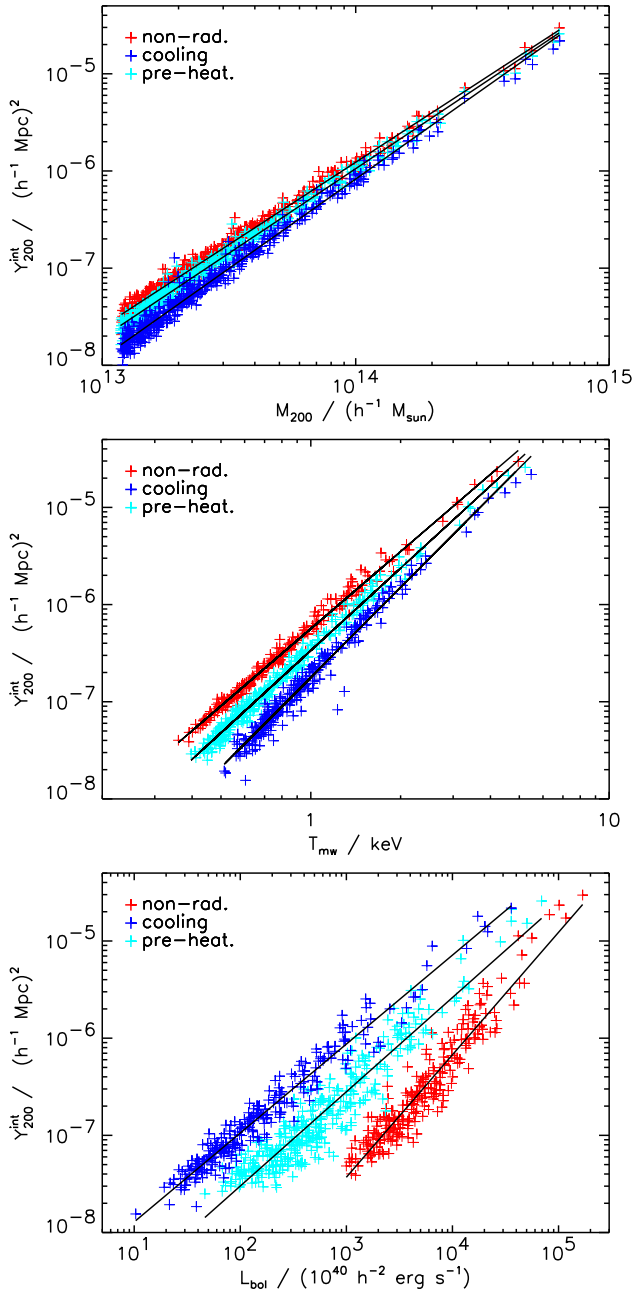

Figure 1. SZ scaling relations for clusters at redshift zero from the non-radiative (gray crosses), cooling (dark gray crosses) and pre-heating (light gray crosses) simulations of the ΛCDM cosmology. From top to bottom we have the scalings of the intrinsic Y-flux with mass, mass-weighted temperature and X-ray bolometric luminosity, respectively. The solid lines are power-law fits to the distributions.

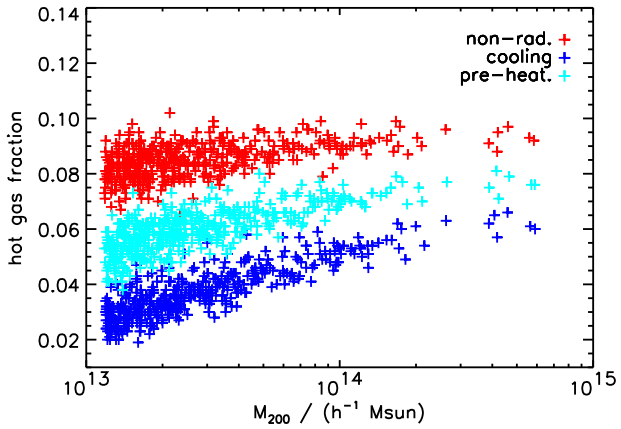

Figure 2. Fraction of hot gas within r_{200} for clusters in the non-radiative (gray crosses) cooling (dark gray crosses) and pre-heating (light gray crosses) simulations.

material forming at the central regions of clusters. As can be inferred from Eq. (7), these are competing effects for the same cluster mass. The overall effect on $Y_{200}^{\rm int}$ is dominated by the decrement of the hot gas mass fraction, which shifts clusters downward in the $Y^{\rm int} - M$ plane. The effect is less strong in the pre-heating run, because particles were heated up by the energy injection mechanism and less amount of cooled material is able to form. The decrement of $Y_{200}^{\rm int}$ is also stronger in low-mass systems, which explains the steepening of the relations.

In Figure 2 we plot $f_{\rm gas}$ for all clusters in non-radiative, cooling and pre-heating catalogues at redshift zero. We see that clusters in the cooling simulation have the lowest hot gas fractions. For low-mass systems these are reduced by about 2.5 times when compared with clusters in the non-radiative simulation. The fraction of hot gas in clusters of the pre-heating run is also substantially reduced, but less than in the cooling case. In both radiative simulations, lower mass systems show lower amounts of hot gas, which implies a lower $Y_{200}^{\rm int}$. In the cooling simulation, this is because cooling becomes more efficient in low-mass systems, where particles have lower temperatures and higher cooling rates due to collisional excitation cooling from neutral elements. In the pre-heating simulation, low-mass systems may also reduce their hot gas fraction in this way. This process is less efficient then in the cooling case because the energy injection rises the temperature of the particles and reduces the contribution from collisional excitation cooling. Pre-heating can also reduce the amount of hot gas in clusters in a different way. Instead of converting hot gas into cooled material, pre-heating has

the effect of heating up and expelling gas from the central regions of clusters. In low-mass systems this may cause some of the hot gas to be expelled from the haloes, which in turn implies lower $f_{\rm gas}$ at lower masses. We find that the amount of baryonic gas which is converted into cooled material in clusters of the cooling and pre-heating simulation can be as high as 50 and 30 per cent, respectively.

The correlation between $Y_{200}^{\rm int}$ and the mass-weighted temperature is also easy to understand. For the same $T_{\rm mw}$, Eq. (7) tells us that the Y-luminosity is simply proportional to the hot gas mass of the cluster. As a consequence, for a given temperature, clusters of the cooling and pre-heating simulations present lower $Y_{200}^{\rm int}$. The effect is again stronger for low-mass systems and for clusters in the cooling simulation. Clusters in the radiative runs also present higher temperatures for the same mass. The combination of these two effects causes clusters to shift in the direction of high temperatures and lower Y-fluxes in the $Y_{200}^{\rm int} - T_{\rm mw}$ plane. The best-fit parameters found for the $Y_{200}^{\rm int} - T_{\rm mw}$ relation are:

Non-radiative: $Y_{200}^{\rm int} = 5.8 \times 10^{-7}\ (T_{\rm mw}/{\rm keV})^{2.6}\ \left(h^{-1}\,{\rm Mpc}\right)^2$

Cooling: $Y_{200}^{\rm int} = 1.8 \times 10^{-7}\ (T_{\rm mw}/{\rm keV})^{3.0}\ \left(h^{-1}\,{\rm Mpc}\right)^2$

Pre-heating: $Y_{200}^{\rm int} = 3.4 \times 10^{-7}\ (T_{\rm mw}/{\rm keV})^{2.8}\ \left(h^{-1}\,{\rm Mpc}\right)^2$

The slopes of the relations derived from the radiative simulations are steeper than those found in the non-radiative run. This is due to the higher temperatures and lower gas masses of clusters in these simulations. Again the non-radiative simulation is in good agreement with the slope 5/2 predicted by the self-similar scaling.

In the top panels of Figure 3 we plot $Y_{200}^{\rm int}$ against the mass-weighted (left panel) and X-ray emission-weighted (right panel) temperatures for clusters in the non-radiative and cooling simulations. These show that the integrated SZ signal presents a much tighter correlation with the mass-weighted temperature than with the emission-weighted temperature. This result confirms expectations, since $T_{\rm ew}$ is weighted by density and temperature and is therefore sensitive to substructures and clumping of the gas inside the cluster. The bottom panels of Figure 3 show the correlation between mass and temperature for the same set of clusters displayed in the top panels. Again, the correlation between M_{200} and $T_{\rm mw}$ presents significantly less scatter than the correlation of M_{200} with $T_{\rm ew}$. This is evidence of the potential of the SZ effect to study the properties of clusters. Future high-resolution SZ observations may provide important constraints on cluster evolutionary theories. Good calibrations of the observed $Y-T$ and $Y-M$ relations may also provide alternative robust estimates of temperature and mass in clusters.

We end the analysis by reporting on the $Y_{200}^{\rm int} - L_{\rm bol}$ correlation. In the radiative runs, the high entropy gas which replaces the cooled material

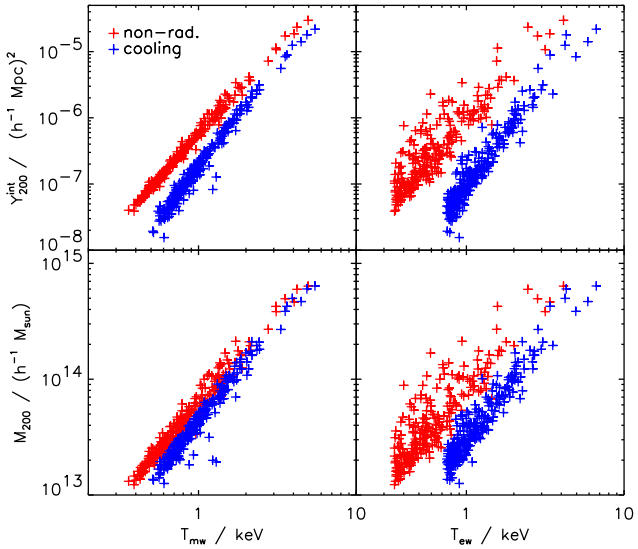

Figure 3. The top panels show the $Y^{\rm int}_{200}$ against the mass-weighted (left panel) and X-ray emission-weighted (right panel) temperatures (respectively $T_{\rm mw}$ and $T_{\rm ew}$) for clusters in the non-radiative (gray crosses) and cooling (dark gray crosses) runs. The bottom panels show mass–temperature correlations for the same set of clusters.

which forms in these simulations is less dense and hotter then the gas in the non-radiative simulation. These variations in temperature and density have opposite effects on the X-ray luminosity, which is a slowly-varying function of temperature, but it is proportional to the square of the gas density, see Eq. (3). As a result, the change in density wins the competition and the luminosity decreases with cooling. The inclusion of pre-heating reduces the amount of cooled material and increases the gas temperature. This implies higher luminosities in the pre-heating run then in the cooling simulation, but lower luminosities than in the non-radiative run. The combination of these effects with the decrease of $Y^{\rm int}_{200}$ explains the substantial shifts observed in the $Y^{\rm int}_{200} - L_{\rm bol}$ relations of Figure 1 in the pre-heating and cooling simulations. The best-fit parameters for the distribution of clusters in the $Y^{\rm int}_{200} - L_{\rm bol}$ plane are:

Non-radiative: $Y^{\rm int}_{200} = 6.3 \times 10^{-12}\ (L_{\rm bol}/L_{40})^{1.3}\ (h^{-1}\,{\rm Mpc})^2$

Cooling: $Y^{\rm int}_{200} = 1.6 \times 10^{-9}\ (L_{\rm bol}/L_{40})^{0.9}\ (h^{-1}\,{\rm Mpc})^2$

Pre-heating: $Y^{\rm int}_{200} = 3.2 \times 10^{-10}\ (L_{\rm bol}/L_{40})^{1.0}\ (h^{-1}\,{\rm Mpc})^2$,

where $L_{40} = 10^{40} h^{-2} {\rm erg\,s^{-1}}$. These show considerable differences of slope and normalization. The slope in the non-radiative run is close to 1.25, which is the value predicted by the self-similar scaling. The

radiative runs show similar slopes, which are less steep than in the non-radiative case. As in the case of the $Y_{200}^{\rm int} - T_{\rm ew}$ relation, the $Y_{200}^{\rm int} - L_{\rm bol}$ relation shows significant scatter due to the sensitivity of the X-ray emission to the density and temperature distribution of the hot gas.

5. Conclusions

We have studied the effect of our models of cooling and pre-heating on the SZ cluster population by identifying clusters in the simulation boxes and computing their characteristic properties. We correlated the SZ luminosity with other cluster properties and derived scaling relations at redshift zero. The non-radiative simulation reproduces well the scalings predicted by the self-similar model, whereas the inclusion of cooling and pre-heating generally changes the slope and normalization of the scaling relations for those runs. The integrated Y-signal is found to be tightly correlated with the mass-weighted temperature and total mass of the cluster.

The author wishes to thank A. Liddle, P. Thomas, S. Kay and O. Muanwong for many fruitful discussions and acknowledges the use of the computer facilities of the Astronomy Unit at Sussex, UK, and CALMIP at Toulouse, France. The simulations used were carried out on a Cray-T3E at EPCC as part of the VIRGO Consortium collaboration.

References

1. Couchman, H. M. P., P. A. Thomas, and F. R. Pearce: 1995. *Ap.J* **452**, 797.
2. da Silva, A. C., S. T. Kay, A. R. Liddle, and P. A. Thomas: 2004 *MNRAS* **348**, 1401.
3. da Silva, A. C., S. T. Kay, A. R. Liddle, P. A. Thomas, F. R. Pearce, and D. Barbosa: 2001. *Ap.J* **561**, L15.
4. Edge, A. C. and G. C. Stewart: 1991. *MNRAS* **252**, 414.
5. Kaiser, N.: 1986. *MNRAS* **222**, 323.
6. Muanwong, O., P. A. Thomas, S. T. Kay, F. R. Pearce, and H. M. P. Couchman: 2001. *Ap.J* **552**, L27.
7. Muanwong, O. and Thomas, P. A. and Kay, S. T. and Pearce, F. R.: 2002. *MNRAS* **336**, 527.
8. Navarro, J. F., C. S. Frenk, and S. D. M. White: 1997. *Ap.J* **490**, 493.
9. Pearce, F. R. and H. M. P. Couchman: 1997. *New Astronomy* **2**, 411.
10. Ponman, T. J., D. B. Cannon, and J. F. Navarro: 1999. *Nature* **397**, 135.
11. Sunyaev, R. A. and Y. B. Zel'dovich: 1972. *Comm. Astrophys. Space Phys.* **4**, 173.
12. Sutherland, R. S. and M. A. Dopita: 1993. *Ap. J.* **88**, S253.
13. Thomas, P. A. and H. M. P. Couchman: 1992. *MNRAS* **257**, 11–31.
14. Xue, Y. and X. Wu: 2000. *Ap.J* **538**, 65.